Thematic Set:
Fault and top seals

PG
Petroleum Geoscience

Published online October 14, 2016 https://doi.org/10.1144/petgeo2016-038 | Vol. 23 | 2017 | pp. 104–119

Do deformation bands matter for flow? Insights from permeability measurements and flow simulations in porous carbonate rocks

Atle Rotevatn[1*], Heidi S. Fossmark[1,3], Eivind Bastesen[2], Elin Thorsheim[1,3] & Anita Torabi[2]

[1] Department of Earth Science, University of Bergen, Norway
[2] Uni Research CIPR, Bergen, Norway
[3] Present address: Statoil, Bergen, Norway
* Correspondence: atle.rotevatn@uib.no

Abstract: We investigate the permeability and flow effects of deformation bands in porous granular carbonate rocks in Malta and use results from flow simulations to discuss the practical implications of deformation bands in carbonate and siliciclastic reservoirs rocks in general. Image- and laboratory-based analyses of deformation bands show permeabilities that are 1 – 2 orders of magnitude lower than the adjacent host rocks. Small-scale outcrop-based flow models (1 × 1 m) focus on the effect of deformation band on flow at the scale of individual bands. Two-phase flow simulations (water displacing oil) show that at the local scale a decrease in deformation band permeability led to increasing flow complexity, reduced and irregular waterfront propagation and reduction in sweep efficiency. A reduction in host rock permeability is associated with increased sensitivity to deformation bands. In low-permeable host rocks, a single magnitude-order reduction of deformation band permeability significantly delays flow, whereas in higher-permeable host rocks the effect is less pronounced. Hence, in some cases, deformation bands may represent a significant impediment to flow already when they are only 1 – 2 orders of magnitude less permeable than host rock. Consequently, deformation bands may have greater practical implications than previously thought, particularly in reservoir rocks with moderate to low host rock permeability.

Received 2 March 2016; **revised** 27 June 2016; **accepted** 4 July 2016

Failure in porous granular rocks may result in the formation of tabular, millimetre-thick zones of localized but non-discrete strain (Friedman & Logan 1973; Engelder 1974) that are generally referred to as deformation bands (Aydin 1978). The most common type of deformation bands is associated with shear and a minor component of compaction; these are referred to as compactive shear bands (Aydin *et al.* 2006) and are the subject of interest in the present study. Deformation bands may accommodate strain through one or more of the following mechanisms:

(i) non-destructive grain reorganization (grain rolling, sliding, 'disaggregation'; Mandl *et al.* 1977; Bense *et al.* 2003; Rawling & Goodwin 2003);
(ii) brittle cataclasis (grain flaking, fracturing and crushing; Aydin 1978; Jamison & Stearns 1982; Aydin & Johnson 1983; Antonellini *et al.* 1994; Lothe *et al.* 2002; Saillet & Wibberley 2010; Rotevatn & Fossen 2012; Fossen *et al.* 2015);
(iii) dissolution and cementation (dissolution, redistribution and precipitation of dissolved material, e.g. through pressure solution; Gibson 1998; Tondi *et al.* 2006; Fossen *et al.* 2007; Cilona *et al.* 2012).

In porous siliciclastic rocks, grain reorganization and brittle cataclasis appear to dominate strain accommodation (e.g. Aydin 1978; Antonellini *et al.* 1994; Rotevatn & Fossen 2012), whereas dissolution and cementation is often secondary and of post-kinematic nature (Gabrielsen & Koestler 1987; Leveille *et al.* 1997; Fisher & Knipe 2001; Fossen *et al.* 2007). Within deformation bands in porous granular carbonate rocks, however, grain-scale dissolution appears to be a primary mechanism for strain accommodation and plays an important role in grain-size reduction (Tondi *et al.* 2006, 2012; Tondi 2007; Cilona *et al.* 2012, 2014; Rustichelli *et al.* 2012).

Deformation bands are of interest in reservoir geology and the assessment of fault-related seal and compartmentalization, since they are generally known to be associated with a bulk reduction in permeability ranging from 1 to 6 orders of magnitude relative to host rock (e.g. Antonellini & Aydin 1994; Taylor & Pollard 2000; Sternlof *et al.* 2004; Fossen *et al.* 2007; Rotevatn *et al.* 2008; Ballas *et al.* 2012). Furthermore, and although deformation bands may function as capillary conduits in the vadose zone (Sigda & Wilson 2003; Cavailhes *et al.* 2009), deformation bands have been reported to introduce capillary seals in subsurface aquifers or reservoirs (Torabi *et al.* 2013). Deformation bands have, therefore, been suspected of causing production problems within siliciclastic subsurface reservoirs (Lewis & Couples 1993; Olsson *et al.* 2004), although this has been difficult to prove given their small-scale nature. In response to this, previous studies have attempted to quantify and simulate the effect of deformation bands on fluid flow dynamics and production performance (Matthäi *et al.* 1998; Sternlof *et al.* 2006; Fossen & Bale 2007; Rotevatn *et al.* 2009, 2013; Rotevatn & Fossen 2011; Zuluaga *et al.* 2016). In general these studies have demonstrated that deformation bands in siliciclastic reservoirs or aquifers may cause (i) perturbed flow patterns, leading to more tortuous fluid flow (Rotevatn *et al.* 2009; Zuluaga *et al.* 2016), (ii) pressure compartmentalization (Rotevatn & Fossen 2011), (iii) improved sweep efficiency (Rotevatn *et al.* 2009; Zuluaga *et al.* 2016), (iv) delayed water breakthrough (Rotevatn *et al.* 2009), (v) anisotropic reservoir flow properties (Sternlof *et al.* 2006), (vi) variable production efficiency (Sternlof *et al.* 2006; Rotevatn *et al.* 2009) and (vii) reduced effective permeability within the reservoir (Fossen & Bale 2007; Rotevatn *et al.* 2013). Nevertheless, many question whether deformation bands have any practical implications in reservoir at all (e.g. Fossen & Bale 2007), particularly since previous studies have stated that deformation bands must be

associated with at least 3 – 4 magnitude-orders of permeability contrast to host rock in order to affect flow noticeably. In this study, we offer new insights to the practical implication of deformation bands based on reservoir modelling and flow simulations at a very small scale. Although this study has a basis in deformation bands occurring in porous granular carbonate rocks, the main findings are equally applicable to siliciclastic reservoirs affected by deformation bands.

Within porous granular carbonate rocks there is a growing body of documentation covering the structure, mechanics and kinematics of natural deformation bands (Tondi *et al.* 2006, 2012; Tondi 2007; Antonellini *et al.* 2008, 2014*b*; Agosta *et al.* 2009; Cilona *et al.* 2012; Rustichelli *et al.* 2012) as well as laboratory-induced deformation bands (Baxevanis *et al.* 2006; Baud *et al.* 2009; Vajdova *et al.* 2010; Zhu *et al.* 2010; Cilona *et al.* 2012, 2014; Ji *et al.* 2015). Studies reporting permeability, on the other hand, are scarce but suggest that deformation bands in carbonate rocks are associated with a permeability reduction of 1 – 3 orders of magnitude relative to host rock (Rath *et al.* 2011; Antonellini *et al.* 2014*a*, *b*; Tondi *et al.* 2016). To date, only one study has attempted to quantify the flow effect of deformation bands in carbonate reservoirs, using numerical simulations of radial drawdown during single-phase flow (Antonellini *et al.* 2014*a*); the authors conclude that zones of compactive shear bands, as well as well-developed sub-seismic faults, may affect flow and have adverse effects on production.

In this study we attempt to expand the knowledge of the impact of deformation bands on fluid flow in porous carbonate rocks and, by extrapolation of flow modelling results, in other porous rocks. To do this, we first present new permeability data from compactive shear bands within grain-supported carbonate rocks. Furthermore, we use two-phase flow simulations (oil production using water drive) of small-scale (1 × 1 m) outcrop-based reservoir models to study the effect of deformation bands on flow dynamics in such rocks, investigating a range of different scenarios where host rock and deformation band permeability are the main variables tested.

It should be noted that the modelling exercise presented in this study is very different from the workflow and philosophy of building a reservoir model of an entire oil field, as is routinely done in the hydrocarbon industry. The modelling effort presented in this paper occurs on a very small scale (1 × 1 m outcrop-based reservoir models) to understand flow at the scale of individual bands, whereas any discussion of implications for flow at a full-field/reservoir scale represent an extrapolation of the learnings made from our modelling results. The reason for generating models at such a small scale is that the key topic of interest here is the effect of deformation bands as small-scale structural heterogeneity. We therefore stress that building a field-scale reservoir model with realistic representation of all geological variables, which is an entirely different exercise, is beyond the scope of this study. The point of the exercise in this study is to investigate and isolate the effect of the bands, an exercise that would not be possible in a field-scale model due to the small-scale nature of the bands, and the fact that other variables would cloud the results. Nevertheless, the exercise is important, since in order to understand flow at a larger scale, we first need to understand how flow is affected at the scale of individual bands.

Specifically, we are interested in the effects of the deformation bands on (i) waterfront propagation and -rugosity, (ii) flow dynamics and tortuosity, (iii) time of flight (i.e. time to water breakthrough) and (iv) sweep efficiency. To do this, we have based this study on outcrops of compactive shear bands hosted in grain-dominated carbonate rocks of the Oligocene–Miocene Globigerina Limestone Formation (Pedley *et al.* 1976; Dart *et al.* 1993) in the hanging wall of the Maghlaq Fault in Malta (Bonson *et al.* 2007). We have previously presented a structural study of these outcrops (Rotevatn *et al.* 2016), which forms the basis for the permeability measurements, reservoir modelling and fluid flow simulations undertaken in the current study.

The findings of this study not only shed new light on the flow effects of deformation bands in grain-dominated carbonate rocks, but bring important and widely applicable new knowledge that elucidates the practical implications of deformation bands in carbonate and siliciclastic reservoir rocks alike.

Study area and previous work

This study uses deformation bands in the hanging wall of one strand of the Maghlaq Fault, Malta (MF; Fig. 1) as the basis for the permeability and flow modelling study presented herein. The MF, described in detail by Bonson *et al.* (2007) and located on the southern coast of Malta (Fig. 1), is a SSW-facing, left-stepping, en echelon normal fault array comprised of relatively straight, 1 – 2 km long, WNW–ESE-trending fault segments linked by shorter (50 – 400 m long) east- to ENE-trending segments. The fault forms part of the shoulder of the WNW-trending Pantelleria Rift (Grasso *et al.* 1986), which formed in late Oligocene to Messinian times (Cello *et al.* 1985) in response to extension localizing between Tunisia and Sicily, likely driven by back-arc north–south-directed extension related to Apennine–Maghrebian shortening (Argnani 1990). The study area is located in the hanging wall of the most east-southeasterly part of the exposed MF, at Ras il-Bajjada (Fig. 1c). The ENE–WSW-trending North Malta Graben and North Gozo Graben dissect the WNW-orientated Pantelleria Rift trend at acute angles of 32° and 66°, respectively and constitute the main structural grain on the islands. These fault trends are considered to be coeval with the Pantelleria rift, having formed under the same, north–south-directed extension (Dart *et al.* 1993), consistent with Argnani (1990). Uplift of the northern rift flank of the Pantelleria Rift, combined with a falling sea-level, caused the emergence of the Maltese archipelago during early Messinian times (Bonson *et al.* 2007).

The stratigraphy of the Maltese islands (Fig. 2) can be subdivided with respect to the Pantelleria rifting event (Pedley *et al.* 1976; Dart *et al.* 1993; Bonson *et al.* 2007) into pre-rift (>21 Ma), early syn-rift (21 – 6 Ma), late syn-rift (<5 Ma) and post-rift deposits (probably <1.5 Ma). (i) The pre-rift strata of the Maltese mainland consists of Lower Coralline Limestone Formation platform carbonates and Lower Globigerina Limestone Member pelagic carbonates. (ii) The early syn-rift strata consists of the Middle to Upper Globigerina Limestone Member (the Middle Globigerina Limestone Member being the interval of interest in this study), as well as the Blue Clay and Greensand formations and the lowermost part of the Upper Coralline Limestone Formation. (iii) The late syn-rift strata is comprised of platform and slope carbonates of the Upper Coralline Limestone and a Plio-Quaternary succession of marls and carbonate mudstones. (iv) The post-rift succession comprises Quaternary to recent hemipelagic and turbiditic muds offshore, and Quaternary talus and alluvial fan deposits onshore.

In our study area in the hanging wall of the MF (Fig. 1), deformation bands are distributed in in a belt of wave-cut platforms and cliff sections over an area *c.* 350 m long and 20 – 30 m wide along the coastline.

Rotevatn *et al.* (2016) recently described the microstructure, kinematics and evolution of the deformation bands in the hanging wall of the Maghlaq Fault; a summary of their key observations is provided here as context for our analysis of permeability and flow effects of the same bands. The host rock to the deformation bands is the Middle Globigerina Limestone Member (MGLM), which in the study area is comprised of bioclastic, grain-supported, porous carbonates (packstones and grainstones) dominated by spherical planktonic foraminifers (mainly globigerinids), elongated bivalve

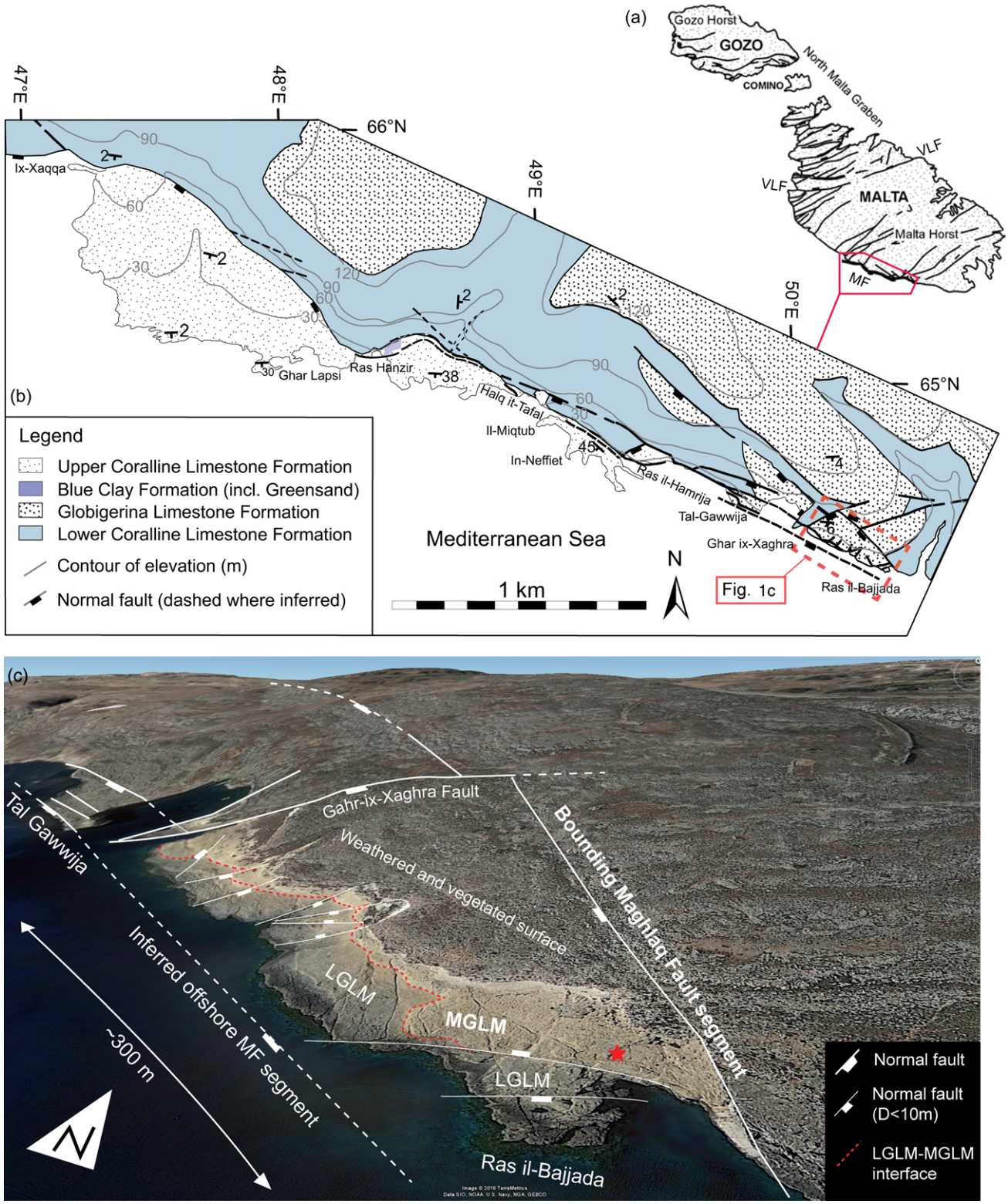

Fig. 1. (**a**) Map showing the location of major normal faults in Malta. MF, Maghlaq Fault; VLF, Victoria Lines Fault. Based on Dart *et al.* (1993) and Bonson *et al.* (2007) and modified from Rotevatn *et al.* (2016). (**b**) Geological map of the Maghlaq Fault, outcropping along 4 km of the southwestern coastline of Malta. Note that individual members of the stratigraphic formations are not distinguished on the map. The topographic contour intervals are in metres above sea level. Location is shown in (a). The study area is located in the WSW, marked by the red polygon and shown in (c). Based on Dart *et al.* (1993) and Bonson *et al.* (2007) and modified from Rotevatn *et al.* (2016). (**c**) Perspective view on to satellite imagery draped on digital elevation model showing the study area on the WSW coastline of Malta. The studied deformation bands are located within the MGLM interval within the fault block bounded by the Gahr ix-Xaghra Fault and the Maghlaq Fault. The location is shown in (b). The red star shows the location of the area shown in Figure 6 which is used in the reservoir models in the present study. No vertical exaggeration. MF, Maghlaq Fault; LGLM, Lower Globigerina Limestone Member; MGLM, Middle Globigerina Limestone Member. Modified from Rotevatn *et al.* (in review); imagery courtesy of Google Earth.

shells and echinoderm fragments. Helium core plug porosimetry indicated a host rock porosity of 17 – 25% (mean porosity 23%), whereas image analysis yielded a greater spread, yielding porosity values in the range of 10 – 31% (Figs 3 and 4a). Two distinctly different types of deformation bands were identified within the MGLM in the hanging wall of the Maghlaq Fault at Ras il-Bajjada:

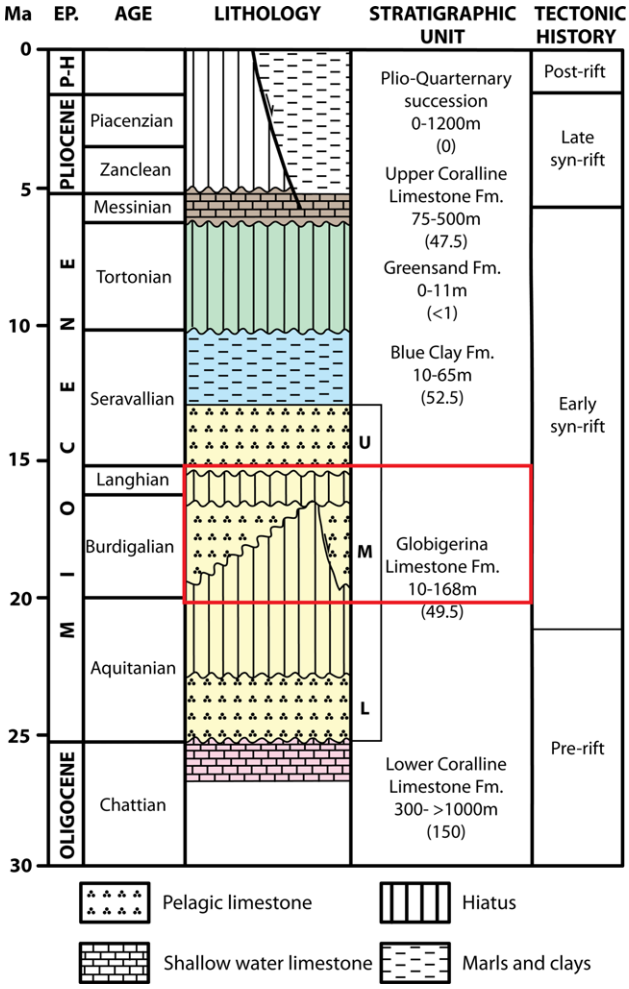

Fig. 2. Tectonostratigraphic log of the Oligocene–Quaternary age sediments of the Maltese archipelago. EP, epoch; P-H, Pleistocene–Holocene. Stratigraphic thickness ranges are based on Pedley (1993) and Bonson *et al.* (2007) and are from onshore Malta, whereas values in brackets indicate local thicknesses along the Maghlaq Fault. The interval of interest is indicated with a red square.

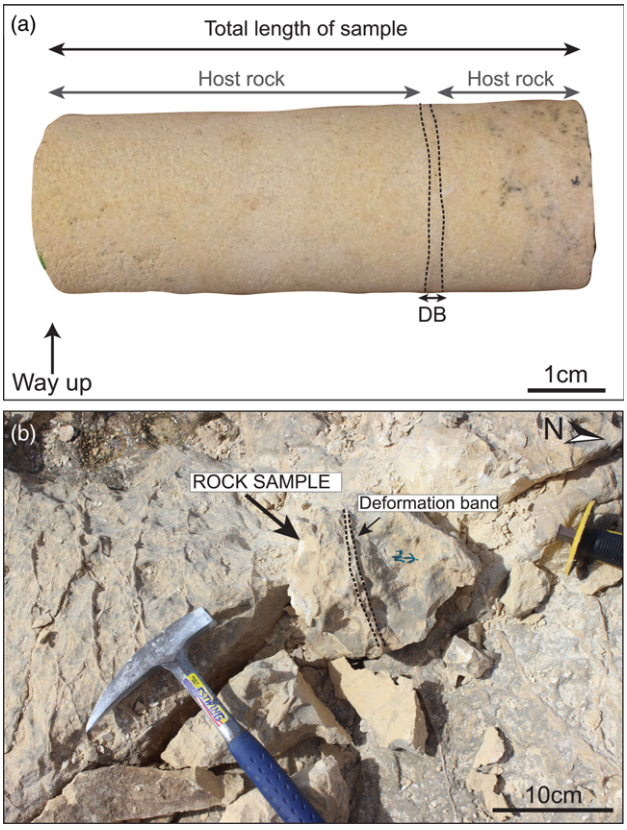

Fig. 3. Overview of sample types collected for thin section and core plug analyses. Core plug example with dimensions is shown in (**a**), whereas a hand sample of a deformation band is shown in (**b**). DB, deformation band.

(i) bed-parallel pure compaction bands (PCBs); and (ii) compactive shear bands (CSBs) orientated at high angle to bedding. Rotevatn *et al.* (2016) demonstrate that PCBs and CSBs formed sequentially during syn-rift sedimentation and growth of the MF during the Pantelleria rifting event (one single tectonic event); PCBs formed first due to early fault-controlled burial in the hanging wall of the MF; CSBs formed subsequently in a perturbed stress field during growth and overlap of MF segments. Microstructural analysis indicates that whereas strain accommodation in PCBs is dominated by grain reorganization and pressure solution, the chief deformation mechanisms responsible for CSB formation are pressure solution and brittle cataclasis. PCBs are rare and of limited lateral extent; their effect on fluid flow is therefore limited and PCBs are not considered further in this study. Instead we focus on the permeability and flow effects of the widely occurring CSBs. Porosity within CSBs was measured to 1 – 8% (mean porosity 3%) based on image analysis of optical photomicrographs, and 5 – 12% (mean porosity 8%) based on image analysis of backscattered electron (BSE) imagery (Fig. 4a). The CSBs occur in outcrop as (i) single bands with thicknesses generally in the range of 1 – 4 mm and, to some extent, as (ii) deformation band clusters comprised of tens of bands and that are up to 20 cm wide, but more commonly as (iii) anastomosing networks, or swarms, ranging from 0.5 to 15 m in width. CSBs are widespread within the MGLM in the study area, with CSB frequency ranging from 4 to 6 CSBs per metre at a distance from faults, but up to *c.* 35 CSBs per metre within anastomosing networks and in the proximity of faults.

From here on we refer to CSBs simply as 'deformation bands'. In order to test the effect of the studied deformation bands on fluid flow at a very fine scale, we select a 1×1 m square within an anastomosing deformation band network for incorporation into a reservoir model that is subsequently subjected to flow simulation. First, however, we investigate the permeability of the studied deformation bands.

Permeability

Methodology

Permeabilities were determined using a combination of image-based and laboratory techniques. Six core plug samples were used for laboratory analysis of permeability within host rock (three core plugs) and deformation bands (three core plugs). Rock samples were collected in the field, taking care to avoid weathered rock by carefully excavating unweathered host rock and deformation bands using a hammer and a chisel. The core plugs were subsequently drilled (from the hand samples) perpendicular to the deformation bands; core plugs have a diameter of one inch (2.54 cm) and range in length from 5.8 to 7.0 cm (Fig. 3). Laboratory measurements of the core plugs were carried out at the Petrophysics Laboratory at the University of Manchester. Gas permeability measurements were obtained by flowing gas through the core plug samples, determining the Klinkenberg-corrected gas permeability by the steady-state technique (Klinkenberg 1941). Note that the resolution of plug measurements is constrained by the plug length and diameter, whereas single deformation bands are only around 1 mm thick (Fig. 3). Thus, laboratory plug measurements represent the effective

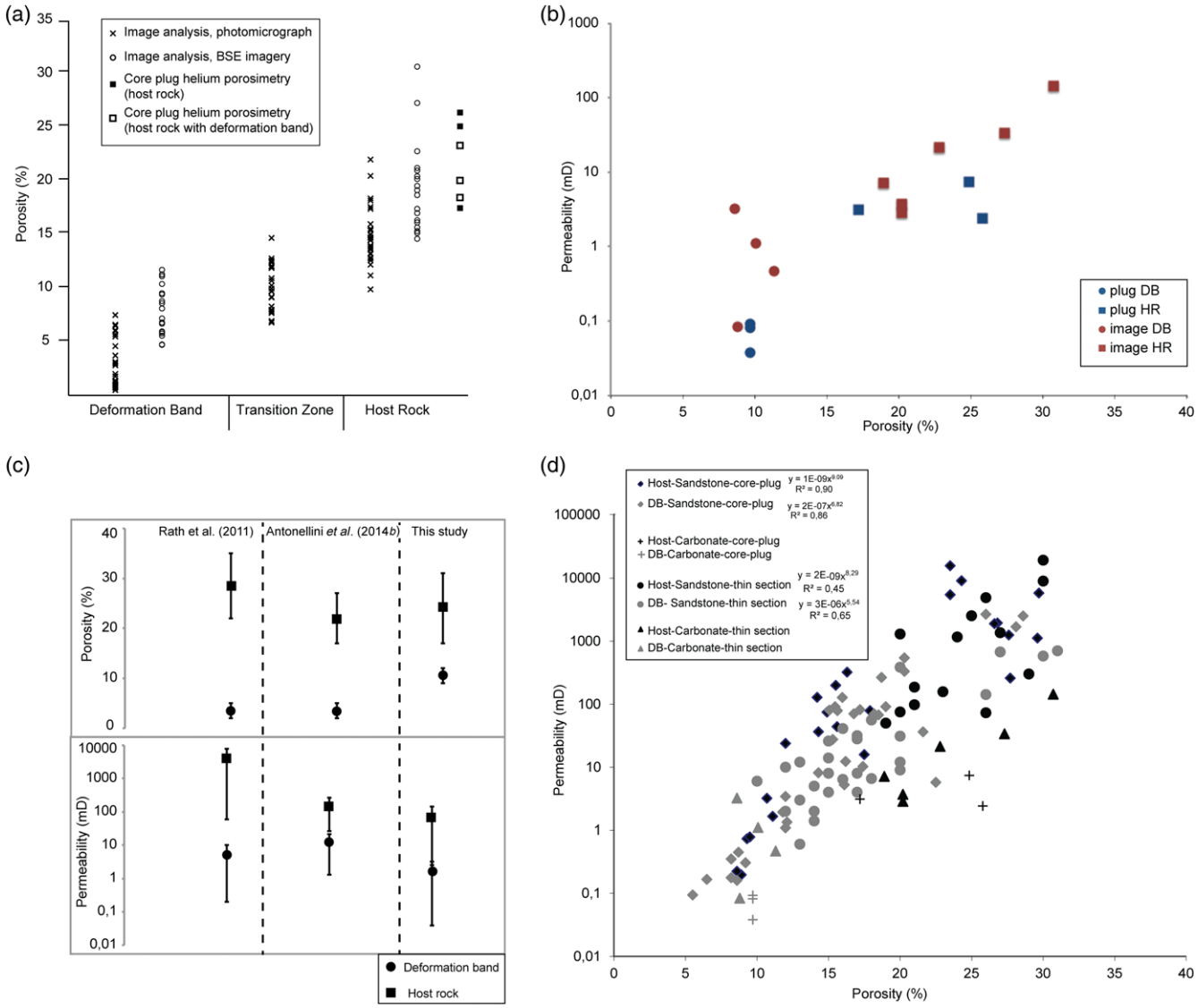

Fig. 4. Porosity and permeability data. (**a**) Porosity data from host rock, deformation bands and transition zones. From Rotevatn *et al.* (2016). (**b**) Permeability data of the present study plotted as a function of porosity. Porosity values plotted were based on the image analyses for deformation bands, and the helium porosimetry for the host rock. (**c**) Comparison of poro-perm data with data from previous studies by Antonellini *et al.* (2014*b*) and Rath *et al.* (2011). (**d**) Porosity–permeability relations in the present study plotted alongside data from sandstones from Torabi *et al.* (2013) for comparison. Note that there is a clear power-law relation between porosity and permeability for sandstone samples. See text for full discussion.

permeability of the whole sample, which includes a deformation band and its host rock. To determine the bulk permeability of the deformation band based on these measurements, a correction based on inverting the harmonic mean was applied, following Deng *et al.* (2015) and using the average host rock permeability derived from the three host rock samples as the basis for the correction.

In addition, permeability estimates using image-based processing of BSE imagery from thin sections (using 1000× magnification) were performed using spatial correlation functions and a modified version of the Kozeny–Carman relation (i.e. relation between grain size and permeability; Torabi *et al.* 2008). In this method, permeability is calculated based on the specific surface area of the pore–grain interface (estimated from a two-point correlation function on binary images) and porosity (estimated from a one-point correlation function on the binary images) as well as formation factor, which is dependent on porosity. This means that both specific surface area as well as porosity can influence the permeability value. As a result of deformation, e.g. cataclasis or pressure-solution processes, the specific surface area of pore–grain interfaces may change and lead to alterations in permeability (see Torabi *et al.* 2008 for a full description of the method). A total of 10 permeability calculations were conducted using this technique: 6 host rock and 4 deformation band calculations (Fig. 4). All of the image-based permeability calculations were conducted on a single thin section, with the purpose to also investigate the spatial variability of permeability within a deformation band and its surrounding host rock (Fig. 5a).

Results

The results from core plug laboratory analyses of gas permeability are shown in Table 1 and Figure 4. Permeability within undeformed host rock core plugs ranges from 2.42 to 7.40 mD, with a mean (arithmetic) of 4.30 mD, whereas calculated deformation band permeabilities range from 0.03 to 0.09 mD, with a mean (arithmetic) of 0.07 mD. Thus, the core plug permeability analyses suggest a permeability reduction of two orders of magnitude within deformation bands relative to host rock. The results from the image-based analyses of permeability are shown in Table 2 and Figure 4; the spatial distribution of permeability measurements is shown in Figure 5a. Image-based permeability within undeformed host rock ranges from 2.86 to 146.66 mD, with a mean of 35.31 mD, whereas

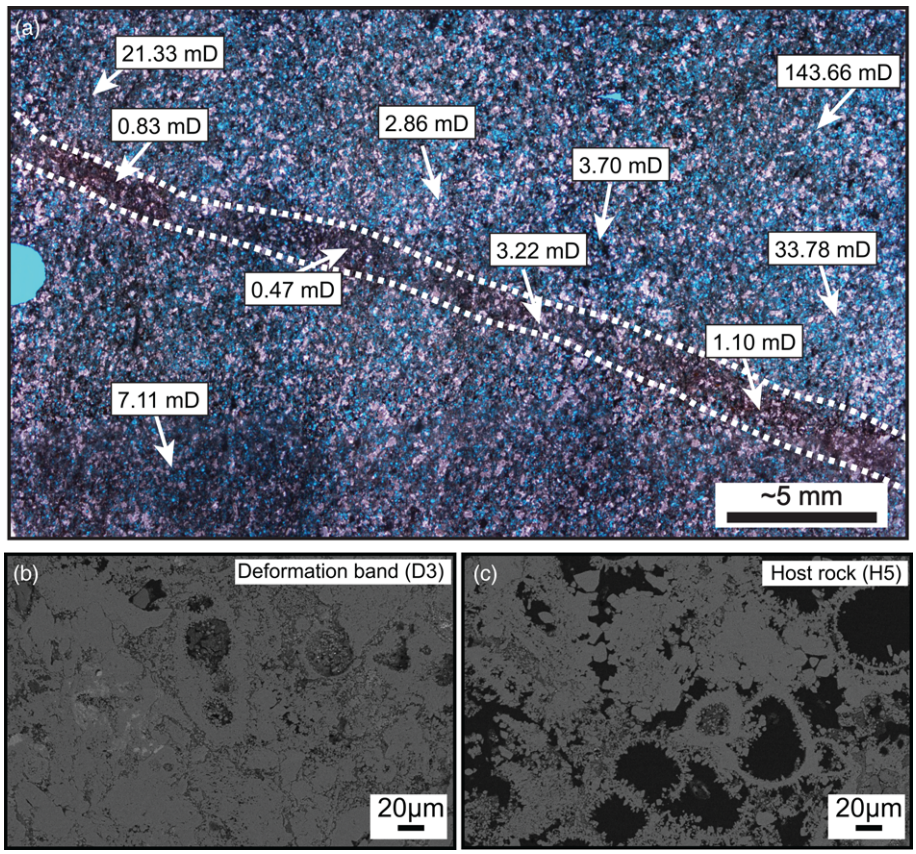

Fig. 5. (**a**) Photomicrograph of deformation band showing the spatial variability of permeability values as determined from image analysis. An overview of the same measurements is shown in Table 2. Arrows indicate where the permeability measurements were conducted; the area sampled varies between each measurement since in each case a minimum representative volume/area needs to be sampled (see Torabi *et al.* (2008) for a full discussion of the method), but is in general in the order of 1 – 2 mm across. (**b**) Backscattered electron (BSE) image from inside the deformation band shown in (a). Note the contrast in porosity (black) compared to the BSE image from the host rock shown in (**c**).

deformation band permeabilities range from 0.47 to 3.32 mD, with a mean of 1.40 mD. Hence, compared to deformation band permeability based on core plug measurements, image analysis yields higher permeabilities by 1 – 2 orders of magnitude. Nevertheless, the permeability calculations obtained from image analysis, reveal 1 – 2 magnitude orders of permeability reduction within the deformation bands relative to the host rock, similar to the permeability contrast obtained from the core plugs.

Reservoir modelling and flow simulation

Approach

We use the industry-standard reservoir modelling software suite Roxar RMS 2012 and its built-in black oil simulator for reservoir modelling and flow simulation in the present study. We have designed an approach that modifies standard reservoir modelling workflows to the needs of the specific problem at hand, and which involves two key strategies: first, the choice of a very fine grid cell resolution to capture the deformation bands and, secondly, 'inflation' of the grid to a scale at which the reservoir modelling software is able to operate. The details of this, which we refer to as a 'semi-discrete inflated approach' to representing deformation bands in a reservoir model, are laid out below.

The aim of the modelling and simulation exercise presented in this paper is to capture the effect of deformation bands on fluid flow at the scale of individual bands, and networks of individual bands, and to use that to assess the practical implications of deformation bands at a larger (reservoir or aquifer) scale. In order to do this, we need to discretely capture the geometry of deformation bands in the grid. This requires a very fine-scaled grid (at a magnitude-order relevant to the millimetre- to centimetre-scale bands) and, therefore, the outcrop pavement area selected for representation in the reservoir model is small (1 × 1 m) in order to make sure the model is computationally feasible despite the fine grid cell size. This is also an ideal domain size to assess the effect of flow at the individual band scale. We therefore select a 1 × 1 m square within an anastomosing deformation band network for incorporation in a reservoir model that is subsequently subjected to flow simulation (Fig. 6). The reason for selecting an area within an anastomosing network is that, since they contain numerous bands and are very continuous, these networks are likely to represent the most significant flow baffles and it is therefore of interest to test them.

The second part of the modelling approach is the 'inflation' of the problem. The software used for the flow simulations is not computationally able to handle the placement of several wells within a distance of less than 1 m from each other. Therefore, we 'inflate' the problem to a domain size of 1 km^2, which is a more

Table 1. *Measured core-plug permeability and calculated deformation band (DB) permeability*

Sample number	Sample length (cm)	Number of DB	Sample permeability (mD)	Thickness range DB (cm)	Min. and max. permeability of DB (mD)	Average permeability of DB (mD)	Host rock permeability (mD)
2	5.80	0	3.12	–	–	–	3.12
11	5.80	0	2.42	–	–	–	2.42
12	6.80	0	7.40	–	–	–	7.40
16	6.30	1	1.02	0.1–0.2	0.020–0.062	0.038	–
37A	7.00	1	1.75	0.05–0.2	0.017–0.205	0.082	–
37B	7.00	4	0.53	0.5–1*	0.048–0.145	0.093	–

*Cumulative thickness, as there are four deformation bands present.

Table 2. *Permeability obtained from image analysis*

Measurement number	Deformation band permeability (mD)	Host rock permeability (mD)
D1	1.10	–
D2	0.467	–
D3	0.832	–
D4	3.230	–
H1	–	2.86
H2	–	3.71
H3	–	33.78
H4	–	143.66
H5	–	21.33
H6	–	7.11

suitable size range for the simulator (Fig. 6c). This leads to the initially 1 × 1 m square becoming 1000 × 1000 m, and inflates grid cells with dimensions of 1 × 1 × 1 cm to become grid cells with dimensions 10 × 10 × 10 m. As part of this, individual deformation band thicknesses (originally 3 mm mean thickness) are 3 m thick in the inflated model. However, since all size relationships are kept constant during inflation (i.e. ratio of deformation band to host rock width/area/volume), this approach is sound for comparing flow behaviour in different models. The model is comprised of a single layer of grid cells, corresponding to a grid cell configuration of 100 × 100 × 1, bringing the total number of cells to 10 000. It is important to stress that this is merely a technical workaround needed to build the model, and that this does not represent any attempt at claiming that the deformation bands are of different dimensions/distribution than in reality. Results are therefore normalized and discussed in the context of the original 1 × 1 m size of the outcrop that formed the basis for the reservoir models.

The detailed technical steps taken in the construction of the reservoir model following this approach are explained in the following section.

Incorporating the deformation band network from outcrop to model

The inflated reservoir model was built as a single layer (10 m thick) orthogonal geocellular grid between two horizontal surfaces measuring 1000 × 1000 m. In order to discretize the deformation bands in the geocellular model, the detailed 1 × 1 m deformation band map shown in Figure 6c was initially imported into RMS, and scaled to fit the model boundaries of 1000 × 1000 m in the *x*- and *y*-directions. With an average grid cell size of 10 × 10 × 10 m, we are able to capture the geometry of individuals or groups of 2 – 4 deformation bands (inflated thickness being 3 m), using a multiplier to factor in the number of bands in each cell (0 – 4). Therefore, using the scaled image, a band frequency parameter was generated for the geocellular grid (Fig. 6d), where a value is assigned to each cell corresponding to the number of deformation bands (0 – 4) in each cell. The model comprises only one layer of cells in the vertical

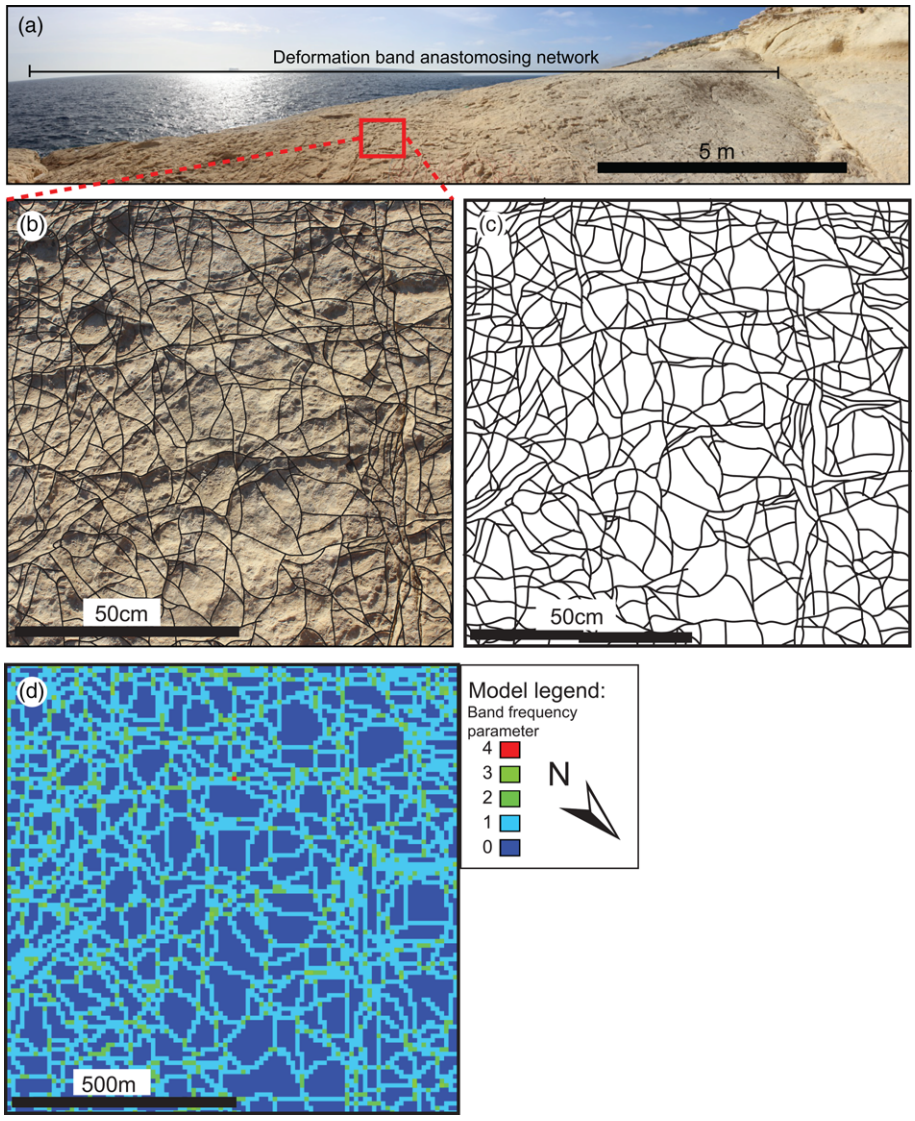

Fig. 6. (**a**) Outcrop of an anastomosing network of deformation bands; see Figure 1c for location indicated by red star. An within the band network (**b**) was selected, and a deformation band map was created (**c**). The deformation band map was used to create a band frequency parameter (**d**) that was used to condition the geocellular reservoir model, incorporating the deformation bands and their permeabilities. The legend shows the value assigned to each cell in the band frequency parameter, which corresponds with the number of deformation bands (0 – 4) in each cell. See text for full discussion.

direction (*z*-axis), based on an assumption/simplification that all deformation bands are sub-vertical and continuous through the model. Modelling the deformation bands as being vertically continuous throughout the model is necessary, since fluids in the simulations would otherwise flow around the band network, and we would then be unable to test the effects of cross-band flow. Given the model choices (1 layer, vertically continuous deformation bands), our approach is largely two-dimensional, which is a fair approximation of flow across a network of bands confined to one geological layer (e.g. Rotevatn *et al.* 2009).

The model resulting from this semi-discrete inflated approach very closely replicates the exact geometry of the deformation band as mapped in outcrop (compare Fig. 6b and d), and is well suited to test the effect of deformation bands on flow at a scale close to that of individual bands.

Assignment of petrophysical properties to the grid

As the main aim is to investigate the effect of deformation bands on fluid flow, measures were taken to isolate these effects. Lithological contrasts were therefore omitted and reservoir sedimentology was modelled as homogeneous, since inclusion of sedimentological reservoir heterogeneity would serve to cloud the results with respect to the effect of the bands. The assignment of petrophysical properties is therefore mainly concentrated on the properties of the bands.

The band frequency parameter forms the basis for assigning petrophysical properties to the grid cells; the main property of interest is permeability of deformation bands and host rock. Initially, models were run using the permeabilities measured in the present study (host rock 4.3 mD and deformation bands 0.07 mD); however, the overall low permeability values led to practical and computational problems, including extremely long simulation run times, fatal software errors and termination of simulations prior to completion. We therefore abandoned this attempt and instead used permeability values from the literature from similar but higher-permeable lithotypes. The relationship between our own permeability measurements and those used in our simulations is shown in Figure 4c; permeability inputs were chosen from a range extending across values reported by Rath *et al.* (2011) and Antonellini *et al.* (2014*b*). In addition to alleviating the said practical simulation problems, our use of a wider range of permeabilities from the literature expands the general relevance of our models (i.e. so that they may be applied to other areas where permeabilities are different). Since permeability is the key control on flow as well as being the main variable tested in the models, porosity is, for simplicity, kept constant throughout the various models: 22% porosity for host rock and 5% porosity for the deformation bands. Two host rock permeability scenarios were chosen, a high-permeable case of 1000 mD, and low-permeable case of 150 mD. For the models with 1000 mD host rock permeability (referred to as HH-cases; Fig. 7), three models were run where deformation band permeability was reduced by 1, 2 and 3 orders of magnitude, respectively (models HH_1ORD, HH_2ORD and HH_3ORD, respectively); in addition, a reference model without deformation bands was run (model HH_REF). Additionally, two models with 150 mD host rock permeability were run (referred to as LL-cases; Fig. 7): one reference model without deformation bands (model LL_REF), and one model where deformation bands were given a permeability one order of magnitude less than that of the host rock (model LL_1ORD). This produces a total of six different scenarios that were modelled and flow simulated; an overview of the different model scenarios is shown in Figure 7. Given that each grid cell may contain a combination of host rock and up to 3 – 4 deformation bands (Fig. 6d), we apply a correction based on the band frequency parameter (which provides information as to how many deformation bands of 3 mm thickness, which equates to 3 m in the inflated models, are present in each cell) and a modified harmonic mean to compute effective grid cell permeabilities (similar to the approach used in Rotevatn *et al.* 2009).

As the current study focuses on permeability-controlled effects of deformation bands on fluid flow, capillary effects are beyond the scope of the study and are thus not considered here.

Flow simulation

Flow simulations were performed using the RMS finite difference, black oil simulator. The flow simulations were based on two vertical water-injection wells and two vertical production wells placed on opposite sides of the inflated model, 800 m apart (see, for instance, Fig. 8). Given the pseudo-2D nature of the simulation approach, these injection and production 'wells' are essentially production/injection 'points' in the model; nevertheless we use the term 'well' throughout. Using water drive to establish flow across the model from west to east, the injection wells (constant injection rates; see Appendix A) were positioned in the western part of the model, and the production wells in the eastern part. As the aim was to investigate the effect of deformation bands on fluid flow, the main variables tested were host rock and deformation band permeability. Other dynamic variables were kept constant between the model runs; the dynamic properties used to condition the models are shown in Appendix A. Simulations were run for a minimum of 35 years, or for as long as it took until water breakthrough occurred in the producing wells. The reservoir was assumed to be initially oil filled (i.e. oil–water contact below the geocellular model).

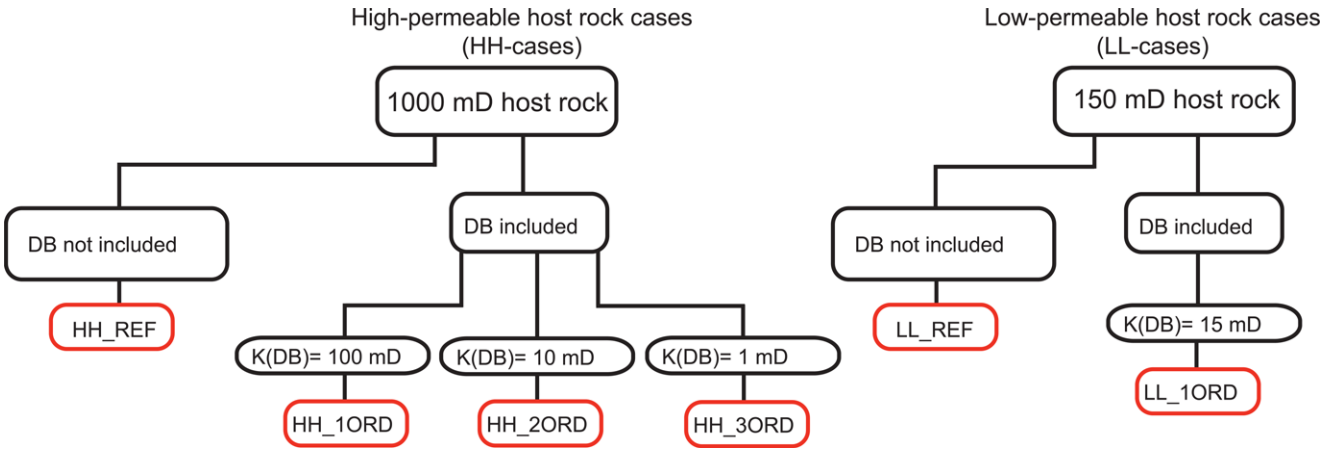

Fig. 7. Hierarchical overview of models built and simulated in this study. Note that the cases are based on the deformation band network shown in Figure 6, but with variable deformation band and host rock permeability. Thus, the cases are effectively different realizations of the same deformation band network but with different host and band permeabilities.

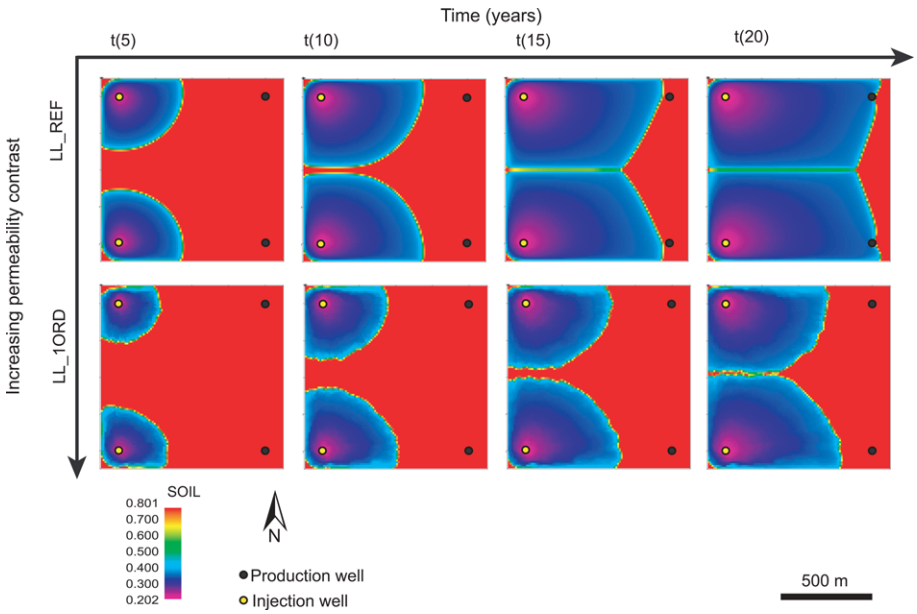

Fig. 8. Simulated production of the low-permeable host rock cases (LL-cases) shown by oil saturation through different time steps; four time steps are shown. Note the placement of injection wells in the western part of the models and production wells in the eastern part of the models. The reference model is shown in the top row, whereas the model with one order of magnitude deformation band permeability reduction is shown at the bottom. The direction of flow is from left to right.

The purpose of the exercise is to use flow simulations as a dynamic test of reservoir response to the presence of structural heterogeneity, and to perform a comparison of different model scenarios. More sophisticated simulation approaches and production optimization are beyond the scope of this study.

Experimental design

Several test simulations were run to identify an optimal set of dynamic properties to condition the models (mainly focusing on flow rates and borehole pressures). Optimal in this context means identifying a set of injection rates and borehole pressures that are able to successfully drive production by injection of water from left to right in the models. The six models that were built (Fig. 7) were then flow simulated and the results were used to address the following questions:

(1) What are the effects of the observed deformation band network on flow through the models (time of flight, time to water breakthrough)?
(2) What are the effects of the deformation bands on the nature of waterfront propagation (smooth v. irregular)?
(3) What are the effects of the deformation bands on flow tortuosity and sweep efficiency?
(4) How does initial host rock permeability affect how models respond to permeability heterogeneity?

Three key simulation parameters were monitored and used in the subsequent analyses of the results: well production rates, water-cut and oil saturation. The results are presented graphically (Figs 8–13) and in table form (Table 3).

Table 3. *Time to water breakthrough (WBT) for production wells in all models*

	Days to WBT		Years to WBT	
Model	SE well	NE well	SE well	NE well
LL_REF	5721	5721	16	16
LL_1ORD	9435	11 200	26	31
HH_REF	883	883	2.5	2.5
HH_1ORD	1187	1430	3	4
HH_2ORD	5236	7944	14	22
HH_3ORD	42 490	63 005	116	173

Note that years are rounded up/down to closest half-year.

Flow simulation results

Note that all models displayed in Figures 8, 11 and 13 are conditioned for permeability using the band frequency parameter shown in Figure 6d (except the reference models without deformation bands, LL_REF and HH_REF). In other words, deformation bands are very much included, even though these are not visible in the figures when displaying oil saturation through time. Therefore, see Figure 6d to understand the deformation band distribution in the models.

It should be noted that in the following results, the breakthrough times referred to throughout the text are from the 'inflated' models (1000 × 1000 m). The absolute values of the breakthrough times therefore have no significance at the scale of the original outcrop (1 × 1 m); however, their relative differences do, and that is why we present these numbers. Readers are therefore cautioned not to place any emphasis on the absolute breakthrough times, but rather focus on the relative differences in breakthrough times.

Low-permeable host-rock cases (LL-cases; 150 mD host rock permeability)

Fluid flow characteristics were compared between the scenario with low permeability contrast between host rock and deformation bands (LL_1ORD; 1 order of magnitude) and the reference case with no deformation bands present (LL_REF), at different time steps, as illustrated in Figure 8.

In the LL_REF case without deformation bands, the water from the injection wells displaces the oil with smooth and radial fluid fronts (Fig. 8). After five years of simulation, the water has migrated nearly halfway across the grid; however, still as two separate fluid fronts. The two fluid fronts are separate throughout the first ten years of the simulation and link up after *c.* 15 years. After 16 years, the injected water reaches the two production wells in the eastern part of the model simultaneously (Table 3 and Fig. 9).

Comparatively, in the LL_1ORD case, where deformation bands one magnitude-order less permeable than host rock are present, the waterfronts are more irregular (Figs 8 and 10) and the water migrates more slowly across the grid. After five years of simulation, the water has migrated *c.* 200 m away from the injection wells and displaces the water with uneven fluid fronts. The water reaches nearly halfway across the grid after ten years, and the fluid fronts begin to amalgamate after 20 years. Water breakthrough occurs after 26 years in the southern production well, whereas the water reaches the production well in the northern part after 31 years (Table 3 and

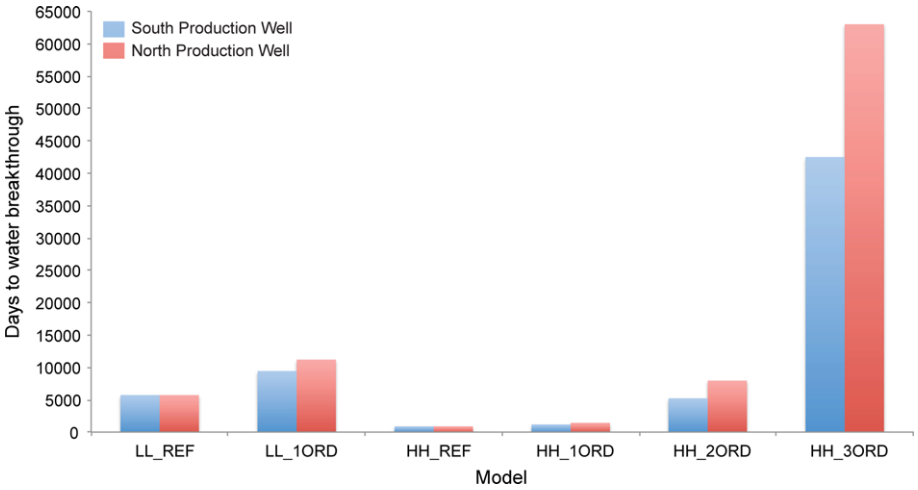

Fig. 9. Time to water breakthrough for the two production wells in the different model runs.

Fig. 9). Thus, with the presence of deformation bands (one order of magnitude less permeable than host rock) in the model, initial water breakthrough is delayed by ten years, representing a 62% increase in time to water breakthrough.

High-permeable host-rock cases (HH-cases; 1000 mD host rock permeability)

Fluid flow characteristics were compared between scenarios with progressively higher permeability contrast between host rock and deformation bands (HH_1ORD, HH_2ORD, HH_3ORD) and the reference case with no deformation bands present (HH_REF), at different time steps, as illustrated in Figure 11.

In the reference case (HH_REF), the waterfront is tabular due to early link-up of the two waterfronts from the injection wells (Fig. 11). Injected water migrates fast in the high-permeable host rock and, within five years of simulation time, the water has nearly saturated the entire grid. Water breakthrough in the two production wells occurs after only 883 days (2.5 years), as shown in Table 3 and Figure 9.

A similar flow pattern is observed in the HH_1ORD case, with just a slightly more irregular front and slightly slower water migration across the grid (Fig. 11). Water breakthrough is reached in southern and northern production wells after three and four years, respectively (Table 3 and Fig. 9). Thus, compared to the reference case (HH_REF), initial water breakthrough is delayed by 0.5 years, representing a 20% increase in time to water breakthrough.

When less permeable deformation bands are introduced (two and three orders of magnitude less permeable than host rock), waterfronts are increasingly uneven with higher degree of tortuosity, and waterfront propagation is increasingly retarded (Figs 11 and 12). For the cases with two (HH_2ORD) and three (HH_3ORD) orders of magnitude permeability reduction relative to host rock, water breakthrough occurs in the southern/northern wells after 14/22 years and 116/173 years, respectively. Compared to the performance of the reference model without deformation bands, this translates to a delay of initial water breakthrough of 12 years and 114 years, respectively, for models HH_2ORD and HH_3ORD. This is equal to an increase in time to water breakthrough of 480 and 4560%, respectively.

Discussion

In this section we focus on (i) the permeability properties of carbonate deformation bands and (ii) the effect of deformation bands on fluid flow in porous rocks based on our simulation models. As we will show below, our flow simulations show many similarities to the findings of previous authors working on flow simulation experiments of deformation bands in porous siliciclastic rocks. However, we also made discoveries that contrasted with the assertions of previous authors, particularly concerning the effect of deformation bands on sweep efficiency and the importance of initial host rock permeability. Note that whereas this work is based on a reservoir model containing deformation bands at a very small scale (model size 1 × 1 m), any discussion of the implications for flow at a reservoir scale represents an extrapolation of the findings from this study.

Permeability of deformation bands in porous carbonates

The permeability values of deformation bands found in the present study largely fall within the range of previously published

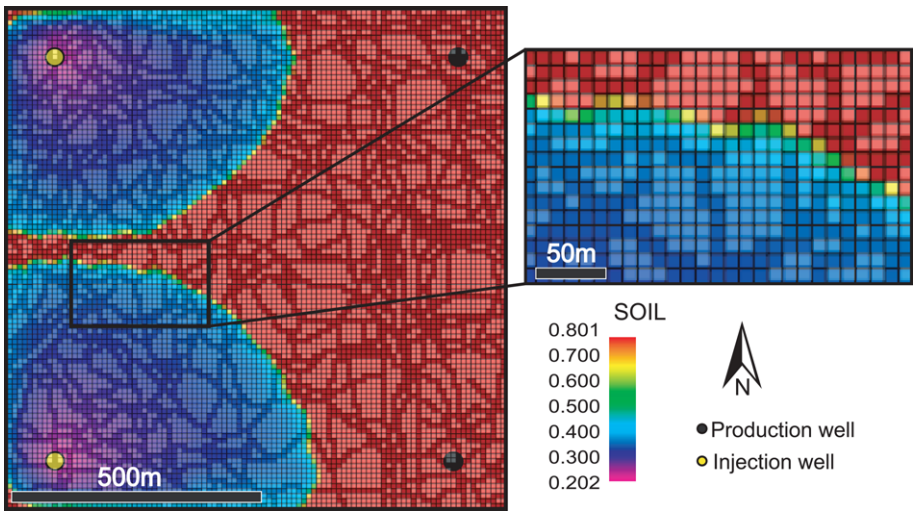

Fig. 10. Diagram showing the local impact of the deformation band network on oil saturation in model LL_1ORD, illustrating the controls of the deformation bands on the nature of waterfront propagation. The direction of flow is from left to right.

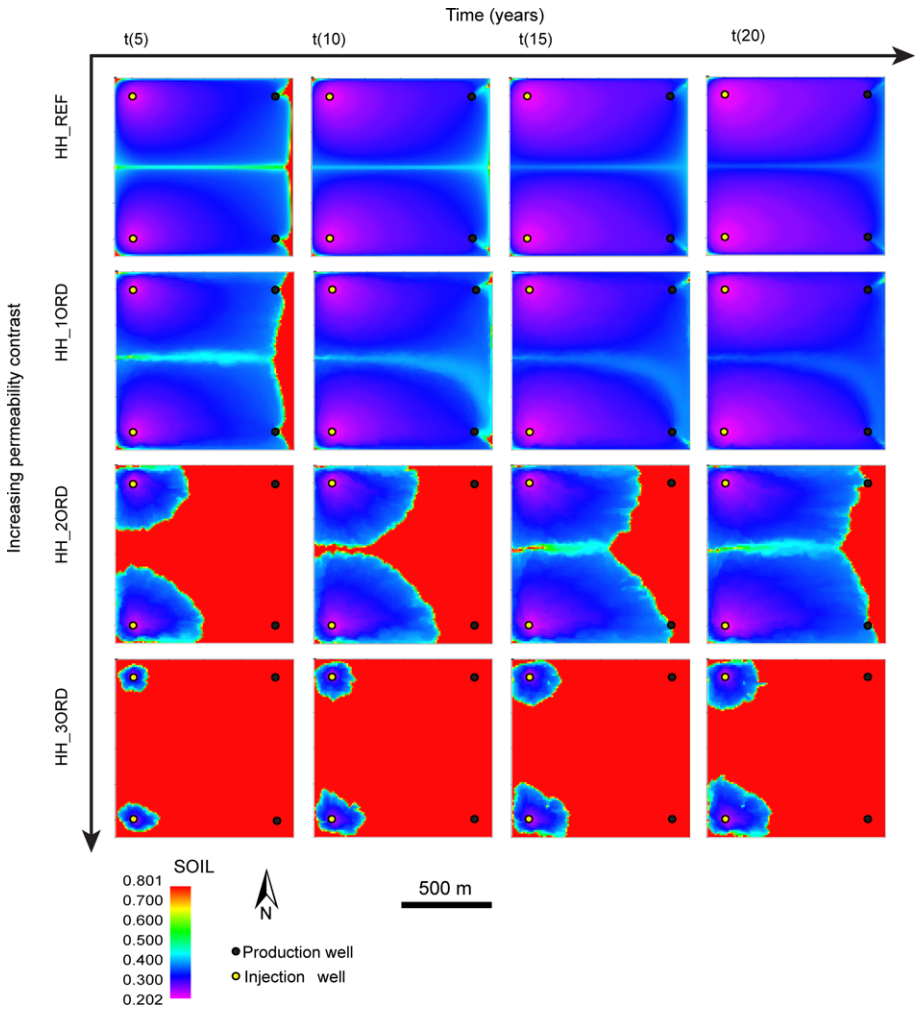

Fig. 11. Simulated production of the high-permeable host rock cases (HH-cases) shown by oil saturation through different time steps; four time steps are shown. Note the placement of injection wells in the western part of the models and production wells in the eastern part of the models. The reference model is shown in the top row, whereas models with progressively higher orders of magnitude (1 – 3) deformation band permeability reduction are shown below. The direction of flow is from left to right.

studies of deformation bands in porous carbonate rocks (Fig. 4c; Rath *et al.* 2011; Antonellini *et al.* 2014*b*). The image-based permeabilities show an internal variability of deformation band and host rock properties. Within the *c.* 20 × 30 mm area show in the image in Figure 5a, host rock permeability varies over two orders of magnitude (2.86 – 146.66 mD), and deformation band permeability varies along strike over one order of magnitude (0.47 – 3.32 mD). Similar variability has been shown for deformation bands in porous sandstones, and Torabi & Fossen (2009) argued that spatial variability of permeability or thickness within deformation bands may reduce their ability to retard flow. Rotevatn *et al.* (2013) tested this assertion and demonstrated that the effects of such variability on aquifer-scale flow are limited; rather, deformation band connectivity as well as permeability contrast were identified as the most important controls on effective permeability and flow.

Figure 4d shows a comparison of the relation between porosity and permeability in sandstone (data from Torabi *et al.* 2013) and carbonate rocks (data from this study) both for host rock and deformation bands. An initial observation is that, overall, the porosity and permeability values for both host rock and deformation band samples are lower for the carbonate rock samples. Based on Torabi *et al.* (2013), there is a clear power-law relation between porosity and permeability for sandstone samples. However, the exponent changes as a function of sample type (host rock or deformation band) and analysis method (image v. core plug; Torabi *et al.* 2008). Currently the amount of data from carbonate rocks is too small to enable a statistically valid fit to those data. However, the visual inspection suggests that it is hard to come up with similar power-law relations for carbonate samples. In other words, predictive use of porosity–permeability relations may be more challenging in porous carbonates compared to sandstones (e.g. Ehrenberg & Nadeau 2005; Lønøy 2006). This may be due to the increased complexity in terms of pore shapes, micro-porosity, cementation etc. in carbonates compared to that of silicilastics.

Deformation band effects on the nature of waterfront propagation

The inclusion of low-permeable flow baffles (deformation bands) in the reservoir models leads to an increasingly heterogeneous permeability distribution in the models. This, in turn, affects the nature of flow and waterfront propagation, leading to increasingly complex flow patterns as permeability of deformation bands is progressively reduced. For example, consider Figure 10, which shows the propagating waterfront in a simulation with low contrast between host and deformation band permeability. Here, waterfront propagation is relatively smooth and the shape of the waterfront is regular. Contrastingly, Figure 12 shows the waterfront in an experiment with high contrast of host and deformation band permeability. Here, the waterfront is more complex and irregular, as a result of the lower-permeable bands. The reason for these differences is that the introduction of permeability heterogeneity in the models results in slower and more irregular waterfront propagation, compared to models where deformation bands are absent. Thus, at the local scale, deformation bands clearly affect flow patterns and the nature of waterfront propagation; similar finds were reported by Rotevatn *et al.* (2013) for arrays of contractional deformation bands in porous siliciclastic rocks.

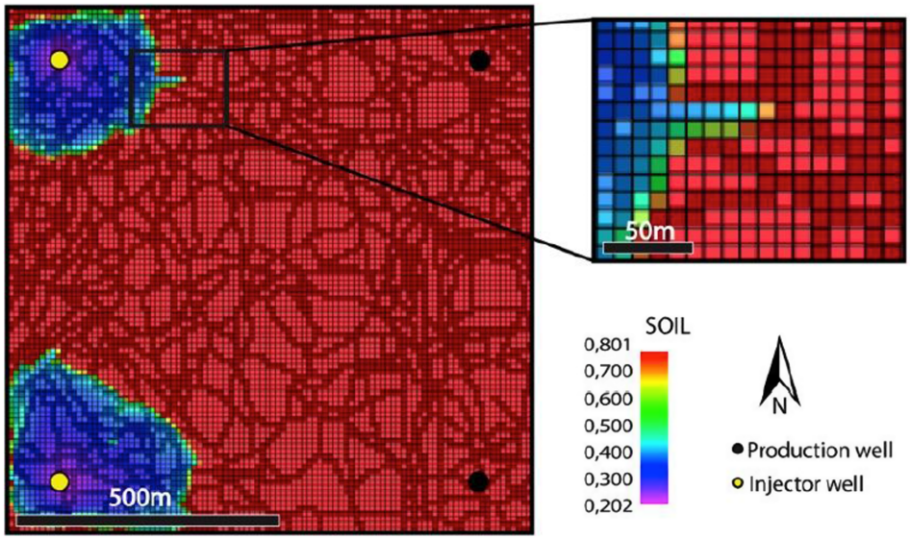

Fig. 12. Diagram showing the local impact of the deformation band network on oil saturation in model HH_3ORD, illustrating the controls of the deformation bands on the nature of waterfront propagation. The direction of flow is from left to right.

Deformation band effects on the speed of flow

Fachri *et al.* (2013), based on flow simulations of larger-scale reservoir models of relay zones in siliciclastics with deformation band damage zones, reported a link between increasingly complex waterfront shapes (as a function of decreasing deformation band permeability) and a decrease in the speed at which fluid fronts propagate. In the present study, although at a much smaller scale, we observe that the models with the more complex fluid propagation fronts are also associated with low rates of fluid propagation. The flow simulations clearly show that even though fluids are able to propagate across the grid in all cases, a progressive decrease in deformation band permeability leads to progressively slower migration of injection fluids from the injector pair to the producer pair (Figs 8 and 11), resulting in increasingly delayed water breakthrough (Fig. 9). The most substantial delay is, as expected, when the deformation bands have three orders of magnitude permeability reduction relative to host rock (HH_3ORD; Fig. 11), causing extreme delays in initial water breakthrough (Fig. 9 and Table 3). However, water breakthrough is delayed in all models where deformation bands are present, also at 1 – 2 orders of permeability reduction relative to host rock.

Effects on sweep efficiency

This discussion concerns sweep efficiency at the scale of the outcrop-based models (1 m^2) of the present study; this is contrasted and compared with results at reservoir/field scale by previous authors, but we caveat that extrapolations to a larger scale should be treated with some caution.

Reservoir sweep efficiency in the different simulated models, i.e. the ability of injected water to saturate the reservoir, is variable and appears to be significantly affected by deformation band permeability. In the reference models without deformation bands, smooth waterfront propagation and a homogeneous permeability field leads to good sweep efficiency throughout the model, as reflected by high water saturation at the end of the simulations (models HH_REF and LL_REF; Fig. 13). There is good pressure communication between the wells, and the water takes a direct route to the production wells. However, when introducing deformation bands in the models, waterfronts become increasingly irregular and flow is perturbed due to the heterogeneous permeability field. Increasing flow tortuosity as a function of decreasing deformation band permeability results in a wide zone of residual oil confined between the waterfronts when they link up (see model HH_2ORD in Fig. 11). This zone of lower water saturation gets wider with decreasing deformation band permeability, and thus reflects local areas of poor sweep (compare HH_REF and HH_2ORD in Fig. 11), similar to the 'shadow zones' of bypassed oil reported by Manzocchi *et al.* (2002). Furthermore, at all time steps in the models containing deformation bands, there are larger amounts of oil in the deformation band models compared to the reference cases without deformation bands (Figs 8 and 11). In sum, this points towards a decrease in sweep efficiency as lower permeable flow baffles in the form of deformation bands are introduced. This contrasts with the findings of other studies (e.g. Rotevatn *et al.* 2009; Zuluaga *et al.* 2016) that have reported that increased flow tortuosity caused by low-permeable deformation bands is associated with improvements in sweep efficiency, based on the fact that flow baffles may force injection fluid to sweep parts of a reservoir that would otherwise be bypassed. This is partly related to the difference in the scale of the problem investigated; whereas the said authors' investigations were on a scale of hundreds of metres to tens of kilometres, this study investigates flow at a much smaller scale (1 × 1 m model size), namely that of individual bands. Nevertheless, our results suggest that deformation bands may reduce the ability of fluids to effectively saturate porous rocks affected by deformation bands; yet, on a larger scale, flow baffles may indeed force fluids to sweep parts of the reservoir that would otherwise be bypassed (e.g. Rotevatn *et al.* 2009; Zuluaga *et al.* 2016).

The practical implications of deformation bands on flow

Despite the fact that deformation bands are known to be associated with a significant reduction in bulk permeability (e.g. Antonellini & Aydin 1994; Antonellini *et al.* 2014*b*), previous studies have argued that deformation band permeability must greatly contrast that of the host rock in order to have any noteworthy effect on fluid flow (e.g. Manzocchi *et al.* 1998; Walsh *et al.* 1998; Fossen & Bale 2007). However, an aspect not included in the considerations of these previous studies is the effect of initial host rock permeability; the flow simulations of the present study use different initial host rock permeabilities and in the following we discuss how this affects the results.

Based on our simulation models, we can compare how host rocks with permeabilities of 150 mD (model LL_REF) and 1000 mD (model HH_REF), respectively, respond to the introduction of deformation bands that are just one order of magnitude less permeable than the host rock (models LL_1ORD and HH_1ORD; Fig. 13). When deformation bands are introduced into the 1000 mD host rock, initial water breakthrough is delayed by 0.5 years, equivalent to a 20% increase in time to water breakthrough (compare HH_REF and HH_1ORD in Table 3 and Figs 9 and 13). However, introducing the deformation bands into the 150 mD host

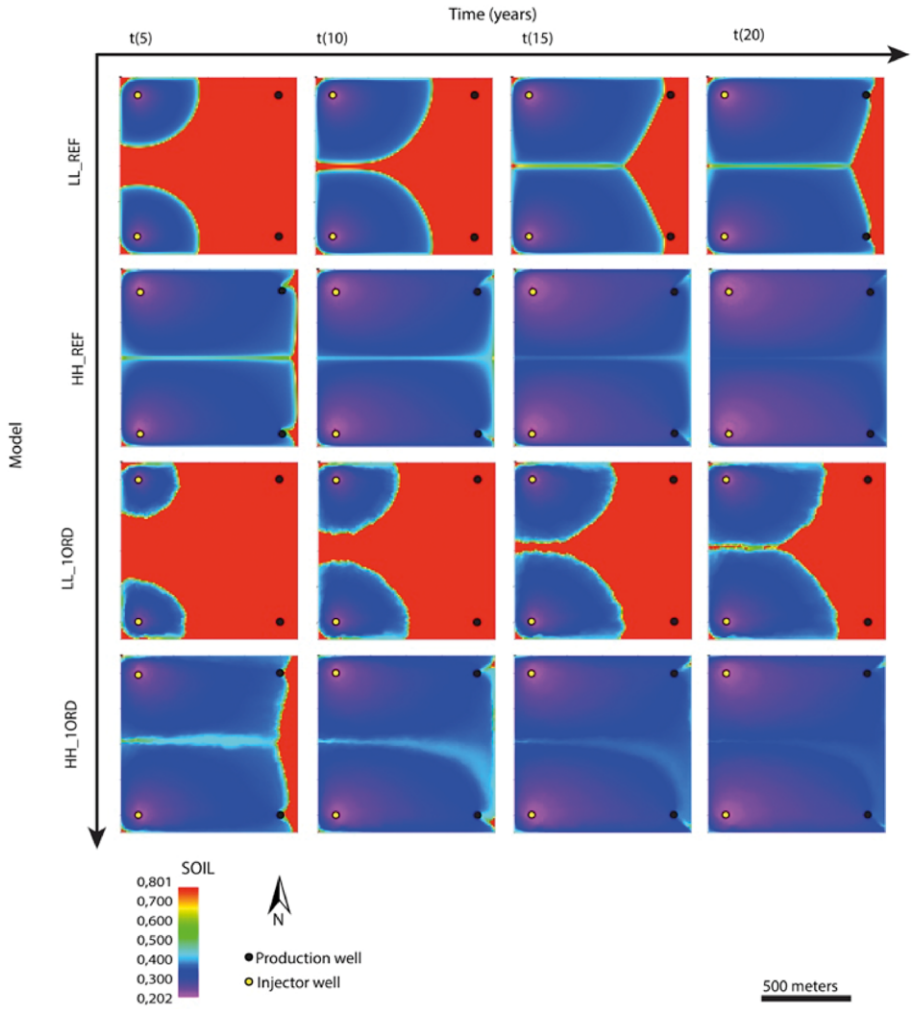

Fig. 13. Oil saturation through four steps of simulated production showing a comparison of how host rock models with high (1000 mD) and low (150 mD) permeabilities respond to the introduction of deformation bands that are one order of magnitude less permeable than the host rock. See text for full discussion.

rock model leads to a ten-year delay in initial water breakthrough, equivalent to a 62% increase in time to water breakthrough (compare LL_REF and LL_1ORD in Table 3 and Figs 9 and 13). These considerations are based on initial water breakthrough, which occurs in the SE production well (Table 3). Water breakthrough occurs somewhat later in the NE production well, and the increase in time to water breakthrough caused by the introduction of deformation bands (one order of magnitude less permeable than host rock) is 60 and 94%, respectively, for the HH and LL cases.

Thus, the low-permeable host rock scenario (LL-cases) appears to be more sensitive to the occurrence of deformation bands with just one order of magnitude reduction in permeability, compared to the high-permeable host rock scenario (HH-cases). This has the important implication that in reservoir rocks of low to moderate host rock permeability, deformation bands may significantly affect flow already when they are only 1 – 2 orders of magnitude less permeable than host rock. This contrasts with the findings of previous authors, who have argued that much higher contrasts are needed: Fossen & Bale (2007) specifically argue, based on mathematical considerations, that deformation bands must exhibit a four magnitude-order contrast in permeability relative to host rock, in order to represent a significant impediment to fluid flow. This was later largely supported by flow simulation studies presented by Rotevatn *et al.* (2009) and Zuluaga *et al.* (2016). However, the finds of the present study suggest that deformation bands with a low permeability contrast to host rock (1 order of magnitude) have a greater flow-retarding effect in models with an initial low to moderate host rock permeability (in this study 150 mD) compared to initially higher-permeable models (in this study 1000 mD). Deformation bands should, therefore, be given due attention as potential flow baffles, particularly in reservoir rocks with low to moderate reservoir properties. Deformation bands are notoriously difficult to image or predict, but where encountered in core, or suspected based on production data, one should pay particular attention to the possibility of deformation-band-related flow baffles near faults (Shipton & Cowie 2003), in folds or at locations of fault interaction (Fossen *et al.* 2005).

Applicability and limitations of the present study

The modelling and flow simulation approaches of the present study have some limitations, the most important of which are listed here. (1) This study does not include capillary effects; including capillary effects would likely amplify the adverse effects on flow exerted by the deformation bands (e.g. Torabi *et al.* 2013) and would therefore not change any of the results herein. (2) The deformation bands are modelled as being vertically continuous through the model; in reality, fluids would be able to flow 'around' the deformation bands in other layers that are more permeable or less affected by deformation bands, and the total reservoir-scale effect of deformation bands on flow would depend on the permeability architecture of the entire reservoir. Nevertheless, the results herein show that deformation bands may have a greater effect on flow than previously thought, and the fact that fluids may flow around arrays of bands does not change that. (3) The flow simulations of the present study are based on water displacing oil; the effect of deformation bands on the flow of gas has not been tested in the present study, but would be an interesting venue for future work. (4) The area modelled in the present study is very small (1 × 1 m); however, the goal of the present study was to test the effect on flow at the scale of individual bands. Reservoir-scale flow modelling is unable to investigate the problem scale of interest in the

present study and is, therefore, out of our scope but has been the focus of several previous studies (e.g. Matthäi *et al.* 1998; Sternlof *et al.* 2006; Rotevatn & Fossen 2011; Zuluaga *et al.* 2016).

Given the overall structural setting of this study, with the studied outcrops located near the intersection of different Maghlaq Fault strands/segments, the most direct analogy to the studied outcrops used is that of a fault intersection setting (compare with, for example, Courthouse Rock, Utah; see Davatzes *et al.* 2005; Fossen *et al.* 2005; Johansen *et al.* 2005). Nevertheless, the overall findings concerning the effects of deformation bands in reservoirs with low initial porosity are considered important regardless of the overall structural setting.

In addition to the above points, it should be noted that the effect of open fractures (joints) is not considered here. This is due to the fact that the studied rocks feature virtually no joints, and the fact that introducing joints in the models would serve to cloud what we are interested in here, namely isolating the effect of deformation bands on flow. One should nevertheless note that in many reservoirs, particularly those with low matrix porosity, joints may significantly increase reservoir permeability, thus countering the effect of low-permeable deformation bands (e.g. Bastesen & Rotevatn 2012; Rotevatn & Bastesen 2014).

Summary and conclusions

The main accomplishments of the present study are twofold. First, we have investigated the permeability of deformation bands in grain-dominated carbonate rocks. Secondly, we have modelled their effect on fluid flow and used the results to discuss the practical implications of deformation bands in subsurface reservoirs or aquifers. The key finds may be summarized as follows.

(1) The permeability of the deformation bands of the present study are 1 – 2 orders of magnitude lower than that of the host rock. Whereas the image-based analysis yield somewhat higher permeability values compared to those based on core-plug laboratory analysis, the two techniques both show a consistent reduction in permeability from host rock to deformation band.
(2) There is significant variability in host rock and deformation band permeability over short distances/areas. Along a single deformation band, permeability varied over an order of magnitude whereas the adjacent host rock varied over two orders of magnitude.
(3) Flow simulations showed that a progressive decrease in deformation band permeability led to (i) increasing delay of water breakthrough, (ii) desynchronized water breakthrough in the two production wells, (iii) perturbed and irregular waterfront propagation; (iv) delayed link-up of the two waterfronts; (v) increasing degree of tortuosity and flow irregularity.
(4) Flow simulations also showed that a reduction in deformation band permeability was associated with a reduction in sweep efficiency. This is due to the fact that the low-permeable bands may reduce the ability of fluids to effectively saturate the affected parts of a reservoir rock.
(5) Low-permeable host rock cases (150 mD host rock permeability) were more sensitive to the presence of deformation bands compared to the higher permeable host rock cases (1000 mD host rock permeability). When compared to reference models without deformation bands, the introduction of deformation bands with one order of magnitude permeability reduction relative to host rock caused a greater increase in time to water breakthrough (in both production wells) in the low-permeable host rock model compared to the high-permeable host rock model.

Our flow simulation work, although initially designed to test the effect of deformation bands in carbonate rocks on fluid flow, has implications relevant for any reservoir with deformation bands, be it siliciclastic or carbonate rocks. These implications are that (i) deformation bands have greater negative effect on flow and, therefore, greater practical implications, in reservoir rocks with moderate to low host rock permeability compared to higher-permeable reservoir rocks; and (ii) deformation bands may, therefore, already represent a significant impediment to flow when they are only 1 – 2 orders of magnitude less permeable than host rock. Thus, the impact of deformation bands on flow should always be considered in the light of the initial host rock permeability, instead of merely as a function of the contrast between host and band permeability.

Acknowledgements and Funding

We are indebted to Chris Bonson and Chris Dart, who generously shared with us their knowledge and experience of Maltese geology at an early stage of this project. Cathy Hollis and Catherine Breislin are thanked for providing the core-plug permeability measurements. Håvard Flatebø Trætteberg is gratefully acknowledged for assistance and company in the field. Charles and Anna Agius are thanked for providing us with a home away in Malta. We thank Roxar for access to academic licences for RMS to the University of Bergen. We are also grateful to Cathy Hollis, Gunnar Sælen and Hilary Corlett for sharing their expertise in carbonate sedimentology. Emma Michie and an anonymous reviewer are acknowledged for their constructive and insightful reviews, which have greatly helped improved the quality of the final manuscript. We are also very grateful to Graham Yielding for his helpful and thorough editorial handling.

Appendix A

Table A1 shows the flow simulation dynamic properties.

Table A1. *Flow simulation dynamic properties*

Length of run	Until water breakthrough in production well	
Other run constraints	Minimum 35 years	
Report step		Every month
Rock/water/oil compressibility		0.0000435 1/bar
Rock reference pressure (bar)		275.79
Oil viscosity (cp)		1.8
Water viscosity (cp)		0.38
Spec. gravity oil		0.8
Gas/oil ratio (Sm^3 Sm^{-3})		142.486
Corey exponents	Water	4
	Oil	3
Saturation end points	S_{ORW}	0.2
	S_{WRC}	0.2
Relative permeability end points	k_{romax}	1
	k_{rw}	0.4
Top of model (m)		0
Oil–water contact (OWC; m)		11
OWC capillary pressure (bar)		0
Reference depth (m)		10
Reference pressure (bar)		50
Wells	Injectors	2
	Producers	2
Flow rate (Sm^3 per day)	Injectors	100 000 (constant)
	Producers	90 000 (target)
Bottom-hole pressure (bar)	Injectors	70 (initial)
	Producers	50 (initial)

References

Agosta, F., Alessandroni, M., Tondi, E. & Aydin, A. 2009. Oblique normal faulting along the northern edge of the Majella Anticline, central Italy: Inferences on hydrocarbon migration and accumulation. *Journal of Structural Geology*, **31**, 674–690.

Antonellini, M. & Aydin, A. 1994. Effect of faulting on fluid flow in porous sandstones: petrophysical properties. *AAPG Bulletin*, **78**, 355–377.

Antonellini, M., Aydin, A. & Pollard, D.D. 1994. Microstructure of deformation bands in porous sandstones at Arches National Park, Utah. *Journal of Structural Geology*, **16**, 941–959.

Antonellini, M., Tondi, E., Agosta, F., Aydin, A. & Cello, G. 2008. Failure modes in deep-water carbonates and their impact for fault development: Majella Mountain, Central Apennines, Italy. *Marine and Petroleum Geology*, **25**, 1074–1096.

Antonellini, M., Cilona, A., Tondi, E., Zambrano, M. & Agosta, F. 2014*a*. Fluid flow numerical experiments of faulted porous carbonates, Northwest Sicily (Italy). *Marine and Petroleum Geology*, **55**, 186–201.

Antonellini, M., Petracchini, L., Billi, A. & Scrocca, D. 2014*b*. First reported occurrence of deformation bands in a platform limestone, the Jurassic Calcare Massiccio Fm., northern Apennines, Italy. *Tectonophysics*, **628**, 85–104.

Argnani, A. 1990. Geophysics of the Mediterranean Basin. The Strait of Sicily rift zone: Foreland deformation related to the evolution of a back-arc basin. *Journal of Geodynamics*, **12**, 311–331.

Aydin, A. 1978. Small faults formed as deformation bands in sandstone. *Pure and Applied Geophysics*, **116**, 913–930.

Aydin, A. & Johnson, A.M. 1983. Analysis of faulting in porous sandstones. *Journal of Structural Geology*, **5**, 19–31.

Aydin, A., Borja, R.I. & Eichhubl, P. 2006. Geological and mathematical framework for failure modes in granular rock. *Journal of Structural Geology*, **28**, 83–98.

Ballas, G., Soliva, R., Sizun, J.-P., Benedicto, A., Cavailhes, T. & Raynaud, S. 2012. The importance of the degree of cataclasis in shear bands for fluid flow in porous sandstone, Provence, France. *AAPG Bulletin*, **96**, 2167–2186.

Bastesen, E. & Rotevatn, A. 2012. Evolution and structural style of relay zones in layered limestone–shale sequences: insights from the Hammam Faraun Fault Block, Suez rift, Egypt. *Journal of the Geological Society, London*, **169**, 477–488, http://doi.org/10.1144/0016-76492011-100

Baud, P., Vinciguerra, S., David, C., Cavallo, A., Walker, E. & Reuschlé, T. 2009. Compaction and failure in high porosity carbonates: mechanical data and microstructural observations. *In:* Vinciguerra, S. & Bernabé, Y. (eds) *Rock Physics and Natural Hazards*. Birkhäuser, Basel, 869–898.

Baxevanis, T., Papamichos, E., Flornes, O. & Larsen, I. 2006. Compaction bands and induced permeability reduction in Tuffeau de Maastricht calcarenite. *Acta Geotechnica*, **1**, 123–135.

Bense, V.F., Van den Berg, E.H. & Van Balen, R.T. 2003. Deformation mechanisms and hydraulic properties of fault zones in unconsolidated sediments; the Roer Valley Rift System, The Netherlands. *Hydrogeology Journal*, **11**, 319–332.

Bonson, C.G., Childs, C., Walsh, J.J., Schöpfer, M.P.J. & Carboni, V. 2007. Geometric and kinematic controls on the internal structure of a large normal fault in massive limestones: The Maghlaq Fault, Malta. *Journal of Structural Geology*, **29**, 336–354.

Cavailhes, T., Soliva, R., Benedicto, A., Loggia, D., Schultz, R.A. & Wibberley, C.A.J. 2009. Are cataclastic shear bands fluid barriers or capillarity conduits? Insight from the analysis of redox fronts in porous sandstones from Provence, France. Paper presented at the European Association of Geoscientists and Engineers 2nd International Conference on Fault and Top Seals, 21–24 September 2009, Montpellier, France.

Cello, G., Crisci, G.M., Marabini, S. & Tortorici, L. 1985. Transtensive tectonics in the Strait of Sicily: Structural and volcanological evidence from the Island of Pantelleria. *Tectonics*, **4**, 311–322.

Cilona, A., Baud, P., Tondi, E., Agosta, F., Vinciguerra, S., Rustichelli, A. & Spiers, C.J. 2012. Deformation bands in porous carbonate grainstones: Field and laboratory observations. *Journal of Structural Geology*, **45**, 137–157.

Cilona, A., Faulkner, D.R. *et al.* 2014. The effects of rock heterogeneity on compaction localization in porous carbonates. *Journal of Structural Geology*, **67**(), 75–93.

Dart, C.J., Bosence, D.W.J. & McClay, K.R. 1993. Stratigraphy and structure of the Maltese graben system. *Journal of the Geological Society, London*, **150**, 1153–1166, http://doi.org/10.1144/gsjgs.150.6.1153

Davatzes, N.C., Eichhubl, P. & Aydin, A. 2005. Structural evolution of fault zones in sandstone by multiple deformation mechanisms: Moab fault, southeast Utah. *GSA Bulletin*, **117**, 135–148.

Deng, S., Zuo, L., Aydin, A., Dvorkin, J. & Mukerji, T. 2015. Permeability characterization of natural compaction bands using core flooding experiments and three-dimensional image-based analysis: Comparing and contrasting the results from two different methods. *AAPG Bulletin*, **99**, 27–49.

Ehrenberg, S. & Nadeau, P. 2005. Sandstone vs. carbonate petroleum reservoirs: A global perspective on porosity–depth and porosity–permeability relationships. *AAPG Bulletin*, **89**, 435–445.

Engelder, J.T. 1974. Cataclasis and the generation of fault gouge. *GSA Bulletin*, **85**, 1515–1522.

Fachri, M., Rotevatn, A. & Tveranger, J. 2013. Fluid flow in relay zones revisited: Towards an improved representation of small-scale structural heterogeneities in flow models. *Marine and Petroleum Geology*, **46**, 144–164.

Fisher, Q.J. & Knipe, R.J. 2001. The permeability of faults within siliciclastic petroleum reservoirs of the North Sea and Norwegian Continental Shelf. *Marine and Petroleum Geology*, **18**, 1063–1081.

Fossen, H. & Bale, A. 2007. Deformation bands and their influence on fluid flow. *AAPG Bulletin*, **91**, 1685–1700.

Fossen, H., Johansen, T.E.S., Hesthammer, J. & Rotevatn, A. 2005. Fault interaction in porous sandstone and implications for reservoir management; examples from Southern Utah. *AAPG Bulletin*, **89**, 1593–1606.

Fossen, H., Schultz, R.A., Shipton, Z.K. & Mair, K. 2007. Deformation bands in sandstone – a review. *Journal of the Geological Society, London*, **164**, 755–769, http://doi.org/10.1144/0016-76492006-036

Fossen, H., Zuluaga, L.F., Ballas, G., Soliva, R. & Rotevatn, A. 2015. Contractional deformation of porous sandstone: Insights from the Aztec Sandstone, SE Nevada, USA. *Journal of Structural Geology*, **74**, 172–184.

Friedman, M. & Logan, J.M. 1973. Lüders' bands in experimentally deformed sandstone and limestone. *GSA Bulletin*, **84**, 1465–1476.

Gabrielsen, R. & Koestler, A.G. 1987. Description and structural implications of fractures in late Jurassic sandstones of the Troll Field, northern North Sea. *Norsk Geologisk Tidsskrift*, **67**, 371–381.

Gibson, R.G. 1998. Physical character and fluid-flow properties of sandstone-derived fault zones. *In*: Coward, M.P., Daltaban, T.S. & Johnson, H. (eds) *Structural Geology in Reservoir Characterization*. Geological Society, London, Special Publications, **127**, 83–97, http://doi.org/10.1144/GSL.SP.1998.127.01.07

Grasso, M., Reuther, C.D., Baumann, H. & Becker, A. 1986. Shallow crustal stress and neotectonic framework of the Malta Platform and the Southeastern Pantelleria Rift (Central Mediterranean). *Geologica Romana*, **25**, 191–212.

Jamison, W.R. & Stearns, D.W. 1982. Tectonic deformation of Wingate Sandstone, Colorado National Monument. *AAPG Bulletin*, **66**, 2584–2608.

Ji, Y., Hall, S.A., Baud, P. & Wong, T.-f. 2015. Characterization of pore structure and strain localization in Majella limestone by X-ray computed tomography and digital image correlation. *Geophysical Journal International*, **200**, 701–719.

Johansen, T.E.S., Fossen, H. & Kluge, R. 2005. The impact of syn-faulting porosity reduction on damage zone architecture in porous sandstone: an outcrop example from the Moab Fault, Utah. *Journal of Structural Geology*, **27**, 1469–1485.

Klinkenberg, L.J. 1941. The permeability of porous media to liquid and gases. In: *Drilling and Production Practice*. *American* Petroleum Institute, New York, 200–213.

Leveille, G.P., Knipe, R. *et al.* 1997. Compartmentalization of Rotliegendes gas reservoirs by sealing faults, Jupiter Fields area, southern North Sea. In: Ziegler, K., Turner, P. & Daines, S.R. (eds) *Petroleum Geology of the Southern North Sea: Future Potential*. Geological Society, London, Special Publications, **123**, 87–104, http://doi.org/10.1144/GSL.SP.1997.123.01.06

Lewis, H. & Couples, G.D. 1993. Production evidence for geological heterogeneities in the Anschutz Ranch East Field, western USA. *In:* North, C.P. & Prosser, D.J. (eds) *Characterization of Fluvial and Aeolian Reservoirs*. *Geological Society, London, Special Publications*, **73**, 321–338, http://doi.org/10.1144/GSL.SP.1993.073.01.19

Lønøy, A. 2006. Making sense of carbonate pore systems. *AAPG Bulletin*, **90**, 1381–1405.

Lothe, A.E., Gabrielsen, R.H., Bjørnevoll-Hagen, N. & Larsen, B.T. 2002. An experimental study of the texture of deformation bands; effects on the porosity and permeability of sandstones. *Petroleum Geoscience*, **8**, 195–207, http://doi.org/10.1144/petgeo.8.3.195

Mandl, G., DeJong, L.N.J. & Maltha, A. 1977. Shear zones in granular material. *Rock Mechanics*, **9**, 95–144.

Manzocchi, T., Ringrose, P.S. & Underhill, J.R. 1998. Flow through fault systems in high-porosity sandstones. *In:* Coward, M.P., Daltaban, T.S. & Johnson, H. (eds) *Structural Geology in Reservoir Characterization*. Geological Society, London, Special Publications, **127**, 65–82, http://doi.org/10.1144/GSL.SP.1998.127.01.06

Manzocchi, T., Heath, A.E., Walsh, J.J. & Childs, C. 2002. The representation of two phase fault-rock properties in flow simulation models. *Petroleum Geoscience*, **8**, 119–132, http://doi.org/10.1144/petgeo.8.2.119

Matthäi, S.K., Aydin, A., Pollard, D.D. & Roberts, S.G. 1998. Numerical simulation of departures from radial drawdown in a faulted sandstone reservoir with joints and deformation bands. *In:* Jones, G., Fisher, Q.J. & Knipe, R.J. (eds) *Faulting, fault sealing and fluid flow in hydrocarbon reservoirs*. Geological Society, London, Special Publications, 157–191, http://doi.org/10.1144/GSL.SP.1998.147.01.11

Olsson, W.A., Lorenz, J.C. & Cooper, S.P. 2004. A mechanical model for multiply-oriented conjugate deformation bands. *Journal of Structural Geology*, **26**, 325–338.

Pedley, H.M., House, M.R. & Waugh, B. 1976. The geology of Malta and Gozo. *Proceedings of the Geologists' Association*, **87**, 325–341.

Pedley, H.M. 1993. Geological Map of the Islands of Malta, 1:25,000 scale. British Geological Survey, Keyworth, UK.

Rath, A., Exner, U., Tschegg, C., Grasemann, B., Laner, R. & Draganits, E. 2011. Diagenetic control of deformation mechanisms in deformation bands in a carbonate grainstone. *AAPG Bulletin*, **95**, 1369–1381.

Rawling, G.C. & Goodwin, L.B. 2003. Cataclasis and particulate flow in faulted, poorly lithified sediments. *Journal of Structural Geology*, **25**, 317–331.

Rotevatn, A. & Bastesen, E. 2014. Fault linkage and damage zone architecture in tight carbonate rocks in the Suez Rift (Egypt): implications for

permeability structure along segmented normal faults. In: Spence, G.H., Redfern, J., Aguilera, R., Bevan, T.G., Cosgrove, J.W., Couples, G.D. & Daniel, J.-M. (eds) *Advances in the Study of Fractured Reservoirs*. Geological Society, London, Special Publications, **374**, 79–95, http://doi.org/10.1144/SP374.12

Rotevatn, A. & Fossen, H. 2011. Simulating the effect of subseismic fault tails and process zones in a siliciclastic reservoir analogue: Implications for aquifer support and trap definition. *Marine and Petroleum Geology*, **28**, 1648–1662.

Rotevatn, A. & Fossen, H. 2012. Soft faults with hard tips: magnitude-order displacement gradient variations controlled by strain softening versus hardening; implications for fault scaling. *Journal of the Geological Society, London*, **169**, 123–126, http://doi.org/10.1144/0016-76492011-108

Rotevatn, A., Torabi, A., Fossen, H. & Braathen, A. 2008. Slipped deformation bands: A new type of cataclastic deformation bands in Western Sinai, Suez rift, Egypt. *Journal of Structural Geology*, **30**, 1317–1331.

Rotevatn, A., Tveranger, J., Howell, J.A. & Fossen, H. 2009. Dynamic investigation of the effect of a relay ramp on simulated fluid flow: geocellular modelling of the Delicate Arch Ramp, Utah. *Petroleum Geoscience*, **15**, 45–58, http://doi.org/10.1144/1354-079309-779

Rotevatn, A., Sandve, T.H., Keilegavlen, E., Kolyukhin, D. & Fossen, H. 2013. Deformation bands and their impact on fluid flow in sandstone reservoirs: the role of natural thickness variations. *Geofluids*, **13**, 359–371.

Rotevatn, A., Thorsheim, E., Bastesen, E., Fossmark, H.S.S., Torabi, A. & Sælen, G. 2016. Sequential growth of deformation bands in carbonate grainstones in the hangingwall of an active growth fault: implications for deformation mechanisms in different tectonic regimes. *Journal of Structural Geology*, **90**, 27–47, http://doi.org/10.1016/j.jsg.2016.07.003

Rustichelli, A., Tondi, E., Agosta, F., Cilona, A. & Giorgioni, M. 2012. Development and distribution of bed-parallel compaction bands and pressure solution seams in carbonates (Bolognano Formation, Majella Mountain, Italy). *Journal of Structural Geology*, **37**, 181–199.

Saillet, E. & Wibberley, C.A.J. 2010. Evolution of cataclastic faulting in high-porosity sandstone, Bassin du Sud-Est, Provence, France. *Journal of Structural Geology*, **32**, 1590–1608.

Shipton, Z.K. & Cowie, P.A. 2003. A conceptual model for the origin of fault damage zone structures in high-porosity sandstone. *Journal of Structural Geology*, **25**, 333–344.

Sigda, J.M. & Wilson, J.L. 2003. Are faults preferential flow paths through semiarid and arid vadose zones? *Water Resources Research*, **39**, http://doi.org/10.1029/2002WR001406

Sternlof, K.R., Chapin, J.R., Pollard, D.D. & Durlofsky, L.J. 2004. Permeability effects of deformation band arrays in sandstone. *AAPG Bulletin*, **88**, 1315–1329.

Sternlof, K.R., Karimi-Fard, M., Pollard, D.D. & Durlofsky, L.J. 2006. Flow and transport effects of compaction bands in sandstone at scales relevant to aquifer and reservoir management. *Water Resources Research*, **42**, W07425.

Taylor, W.L. & Pollard, D.D. 2000. Estimation of in-situ permeability of deformation bands in porous sandstone, Valley of Fire, Nevada. *Water Resources Research*, **36**, 2595–2606.

Tondi, E. 2007. Nucleation, development and petrophysical properties of faults in carbonate grainstones: Evidence from the San Vito Lo Capo peninsula (Sicily, Italy). *Journal of Structural Geology*, **29**, 614–628.

Tondi, E., Antonellini, M., Aydin, A., Marchegiani, L. & Cello, G. 2006. The role of deformation bands, stylolites and sheared stylolites in fault development in carbonate grainstones of Majella Mountain, Italy. *Journal of Structural Geology*, **28**, 376–391.

Tondi, E., Cilona, A., Agosta, F., Aydin, A., Rustichelli, A., Renda, P. & Giunta, G. 2012. Growth processes, dimensional parameters and scaling relationships of two conjugate sets of compactive shear bands in porous carbonate grainstones, Favignana Island, Italy. *Journal of Structural Geology*, **37**, 53–64.

Tondi, E., Rustichelli, A. *et al.* 2016. Hydraulic properties of fault zones in porous carbonates, examples from central and southern Italy. *Italian Journal of Geosciences*, **135**, 68–79.

Torabi, A. & Fossen, H. 2009. Spatial variation of microsturcture and petrophysical properties along deformation bands in reservoir sandstones. *AAPG Bulletin*, **93**, 919–938.

Torabi, A., Fossen, H. & Alaei, B. 2008. Application of spatial correlation functions in permeability estimation of deformation bands in porous rocks. *Journal of Geophysical Research*, **113**, http://doi.org/10.1029/2007JB005455

Torabi, A., Fossen, H. & Braathen, A. 2013. Insight into petrophysical properties of deformed sandstone reservoirs. *AAPG Bulletin*, **97**, 619–637.

Vajdova, V., Zhu, W., Natalie Chen, T.-M. & Wong, T.-f. 2010. Micromechanics of brittle faulting and cataclastic flow in Tavel limestone. *Journal of Structural Geology*, **32**, 1158–1169.

Walsh, J.J., Watterson, J., Heath, A.E. & Childs, C. 1998. Representation and scaling of faults in fluid flow models. *Petroleum Geoscience*, **4**, 241–251, http://doi.org/10.1144/petgeo.4.3.241

Zhu, W., Baud, P. & Wong, T.-f. 2010. Micromechanics of cataclastic pore collapse in limestone. *Journal of Geophysical Research: Solid Earth*, **115**, B04405, http://doi.org/04410.01029/02009JB006610

Zuluaga, L.F., Rotevatn, A., Keilegavlen, E. & Fossen, H. 2016. The impact of deformation bands on simulated fluid flow within fault-propagation fold trap types: lessons from the San Rafael Monocline, Utah (USA). *AAPG Bulletin*, **100**, http://doi.org/10.1306/04151614153